Biosensors and Bioelectronics 242 (2023) 115713

Contents lists available at ScienceDirect

Biosensors and Bioelectronics

journal homepage: www.elsevier.com/locate/bios

Serotonin: A new super effective functional monomer for molecular imprinting. The case of TNF-α detection in real matrix by Surface Plasmon Resonance

Federica Battaglia [a], Francesca Torrini [b], Pasquale Palladino [a], Simona Scarano [a,*], Maria Minunni [a]

[a] Department of Chemistry "Ugo Schiff", University of Florence, 50019, Sesto Fiorentino, FI, Italy
[b] Department of Chemistry and Applied Biosciences, ETH Zurich, Ramistrasse 101, 8092, Zurich, Switzerland

ARTICLE INFO

Keywords:
Molecularly imprinted bio-polymers
Polyserotonin
Polydopamine
Polynorepinephrine
Tumor necrosis factor-alpha
Surface Plasmon Resonance

ABSTRACT

Molecular imprinting and related technologies are becoming increasingly appreciated in bioanalysis and diagnostic applications. Among the imprinted polymers, we have already demonstrated that the endogenous neurotransmitters (NTs) dopamine (DA) and norepinephrine (NE) can be efficiently used as natural and sustainable monomers to straightforwardly design and synthesize a new generation of green and "soft" Molecularly Imprinted BioPolymers (MIBPs). Here, we demonstrated for the first time the ability of a further NT, i.e., serotonin (SE), in forming adhesive imprinted nanofilms coupled to label-free optical biosensing. Its imprinting efficiency is compared with those obtained with PDA and PNE. As a model study, tumor necrosis factor-alpha (TNF-α) was selected as a biomolecular target of interest in clinical diagnostics. The biomimetic receptor was coupled to Surface Plasmon Resonance (SPR), and TNF-α detection was performed in label-free and real-time manner both in buffer and biological matrices, i.e. synovial fluid and human serum. The results indicate that, under the same imprinting and binding conditions, the analytical performances of PSE are impressively superior to those of PDA and PNE. The PSE-based MIBP was able to detect TNF-α in human matrices with a good sensitivity, selectivity, and repeatability.

1. Introduction

The replacement of antibodies (Abs) with mimetic entities in bioanalytical chemistry, diagnostics, and immune-based therapeutics represents an important goal for the scientific community and for ethical reasons, as described by the 2010/63/EU Directive on the protection of animals used for scientific purposes, which asks to limit their use for Abs production only "where a non-animal alternative does not exist" (Directive, 2010/63/EU of the European Parliament and of the Council, 2010). However, the technologies up to now available for Animal-Friendly Affinity (AFA) reagents production did not lead to a decisive turning point, and Abs remain almost the only choice to address most of the (bio)analytical issues based on biomolecular recognition. Among possible alternatives, mimetic receptors appear promising, ideally guaranteeing high stability and long shelf-life, reduction of batch-to-batch variability and cost production, also covering the need for receptors against toxic and non-immunogenic targets.

Strongly convinced by our recent results (Baldoneschi et al., 2020a, 2020b; Battaglia et al., 2021, 2023; Palladino et al., 2018, 2019; Torrini et al., 2021, 2022a, 2022b, 2023a, 2023b) we have great expectations about green and "soft" Molecularly Imprinted Bio-Polymers (MIBPs) (differing from the first generation of "hard" polymers classically named MIPs) obtained from the spontaneous polymerization of the endogenous neurotransmitters (NTs) dopamine (DA) and norepinephrine (NE) as adherent nanofilms. We demonstrated that polydopamine (PDA) and polynorepinephrine (PNE) can be efficiently imprinted both via "whole molecule" and "epitope-based" approaches against a plethora of peptides and proteins leading to robust biomimetic receptors. We coupled these promising and bio-inspired materials both to biosensing by Surface Plasmon Resonance (SPR) and to optical detection on 96-well microplates for ELISA readers (Baldoneschi et al., 2020b; Battaglia et al., 2021, 2023; Palladino et al., 2018; Torrini et al., 2021, 2022a, 2022b,

* Corresponding author.
E-mail addresses: federica.battaglia@unifi.it (F. Battaglia), francesca.torrini@chem.ethz.ch (F. Torrini), pasquale.palladino@unifi.it (P. Palladino), simona.scarano@unifi.it (S. Scarano), maria.minunni@unifi.it (M. Minunni).

https://doi.org/10.1016/j.bios.2023.115713
Received 3 July 2023; Received in revised form 7 September 2023; Accepted 26 September 2023
Available online 30 September 2023

2023a, 2023b). To expand our knowledge on NTs-derived MIBPs for bioanalytical purposes, a new potential functional monomer, serotonin (SE), is proposed here for the first time. Aside from its involvement in important physiological processes, its ability in forming the related bio-inspired polymer (polyserotonin, PSE) is still virtually absent in the literature, excluding only a few recent works (Ishino et al., 2022; Jeon et al., 2021, 2022; Kiratitanavit et al., 2019; Meng et al., 2022; Nakatsuka et al., 2018) that emphasize its potential in various aspects. PSE promises to possess features similar and/or complementary to PDA and PNE and deserves to be further investigated for possible applications in bioanalysis. It is important to highlight that, although PSE is characterized by a similar zeta potential to PDA (−45 mV vs −40 mV, respectively), it displays a marked reduction (ca. 35%) of the unspecific surface interaction with plasma proteins under biological conditions compared to PDA, likely due to lower surface adhesion (Nakatsuka et al., 2018), lower critical surface tension, and higher hydrophilicity (Ishino et al., 2022). These features represent key issues for application of MIBPs in bioassays targeting analytes in complex biological matrices, i.e. serum, plasma, synovial fluid, etc. The great interest in expanding the knowledge about imprinted NTs-based biopolymers is supported by an impressive list of benefits deriving from their use in place of both classic antibodies and "hard" MIPs of the previous generation. Summarizing, their production is extremely low cost and fully water-based, avoiding toxic by-products release typical of classic MIPs; it is achieved in a few hours (up to 5 h), at room temperature, in a single preparation step consisting in the deposition of small volumes (1–200 μL) of the monomer solution containing the template (peptide or protein) on the substrate to be coated (Baldoneschi et al., 2020b; Battaglia et al., 2021, 2023; Torrini et al., 2021, 2022a, 2022b, 2023a, 2023b), leading to homogeneous and self-adherent nanofilms on almost any surface (Baldoneschi et al., 2020a; Jeon and Kang, 2013; Lee et al., 2007; Palladino et al., 2019; Ryu et al., 2018; Torrini et al., 2022b; Xie et al., 2020; Zaidi, 2019). Moreover, they are also temperature resistant, reusable (from tens to ca. a hundred independent measurements), tunable in thickness (from a few nanometers to micrometers), shape, and optical properties. Taken together, all these features lead to a new and extremely promising family of functional monomers of natural origin, fully biocompatible and biodegradable, that allow to achieve the complete greenification of the molecular imprinting process (Arabi et al., 2021; Madikizela et al., 2018; Martín-Esteban, 2013; Ostovan et al., 2022).

To the best of our knowledge, no one has attempted the molecular imprinting of PSE coupled to biosensing for bioanalysis so far, therefore we investigated here, for the first time, its ability in forming adhesive imprinted nanofilms for TNF-α detection via Surface Plasmon Resonance (SPR). TNF-α, here taken as a biological case study, is a target of great interest in clinical diagnostics. It is a cytokine that plays a key role in pro-inflammatory and pro-apoptotic signalling cascades (Horiuchi et al., 2010). Secreted as a monomeric subunit (MW = 17.3 kDa) by activated macrophages and monocytes, non-covalent interactions hold the monomeric subunits together to form a soluble active homotrimer (MW = 51.0 kDa) in solution during inflammation (Horiuchi et al., 2010; Idriss and Naismith, 2000). In this context, several studies have investigated the dynamics of TNF-α monomerization as well as its re-trimerization, showing that the spontaneous transition into an inactive form is a dynamic and fully reversible process that might be altered by therapeutic antibodies and peptides to suppress inflammation (Checco et al., 2020; Corti et al., 1992; Daub et al., 2020; Hlodan and Pain, 1995; van Schie et al., 2016). TNF-α is also an important biomarker, since it is significantly upregulated at intra-articular and systemic level in a multitude of different autoimmune conditions and may, to some extent, reflect disease activity (Popa et al., 2007; Santos Savio et al., 2015; Vasanthi et al., 2007). In this scenario, an accurate determination of this cytokine is mandatory in some diseases and the development of fast and simple detection methods to quantify the concentration of TNF-α represents a challenging task. Nowadays, classical immunoassays (principally ELISA), based on different types of signals recorded, signal amplification strategy, and platform adopted, are the most widely used methods for TNF-α determination in liquid biopsies, mainly serum (Chiswick et al., 2012; Jones and Singer, 2001; Kartikasari et al., 2021; Wang et al., 2006). Nevertheless, several studies show that just a few assays have satisfactory analytical performances in terms of specificity, accuracy, precision, and sensitivity (Breen et al., 2011; Dupuy et al., 2013; Nechansky et al., 2008; Valaperti et al., 2020). Moreover, the correlation between the different immunoassays is almost absent (Valaperti et al., 2020). Behind ELISA assays, biosensor-based approaches have also been proposed, mainly electrochemical (Filik and Avan, 2020; Ghosh et al., 2018; Jeong et al., 2013; Kartikasari et al., 2021; Li et al., 2021; Lu et al., 2021; Yang et al., 2023). The clinically relevant levels of TNF-α in human serum cover a wide range of concentrations spanning from low pmol L^{-1} range, in conditions such as rheumatoid arthritis (RA) or cardiovascular lesions, up to high levels (low nanomolar range) found in patients with sepsis (Damas et al., 1989; El-Kattan et al., 2022; Liu et al., 2021; Oliver et al., 1993). Here, we report the development of "soft" MIBPs for the detection of TNF-α to explore their potential use as an alternative to classical antibodies. Based on our knowledge, only two studies are reported on MIPs for TNF-α detection, both based on a classic methacrylate "hard" polymer, with application in electrochemical sensing (Balayan et al., 2022) and therapeutics (Arad-Yellin et al., 2023) via protein-imprinted polymeric nanoparticles (NPs). The analytical performances of PSE-based MIBPs here developed have been compared, by SPR analysis, to those obtained by PDA and PNE-based ones under the same imprinting and binding conditions. The sensing efficiency of the new PSE-based MIBP biosensor for TNF-α detection has been investigated first in standard conditions, displaying an impressive improvement in the analytical performances, mainly in the dynamic range (ca. 8 and 3 folds, respect to PNE and PDA). Also, the selectivity was evaluated both as α factor (against the real matrix and its interfering proteins) and Imprinting Factor, IF (against non-imprinted PSE), resulting in excellent values. PSE-based MIBP for TNF-α was further tested in real human matrices, i.e., serum and synovial fluid, achieving sensitivities in the low picomolar range for human serum (21 ± 4 pmol L^{-1}) and in the low nanomolar range for synovial fluid (4.5 ± 0.6 nmol L^{-1}), with an excellent reproducibility ($_{av}$CV% = 1.5% and 2.8%, respectively).

2. Materials and methods

2.1. Reagents and chemicals

Tumor Necrosis Factor-alpha (TNF-α) (MW = 17352.7 Da) and the relative synthetic peptide used for the epitope imprinting (residues = 1–11; sequence = VRSSSRTPSDK; MW = 1218.33 Da) were purchased from GenScript Biotech Corporation (Leiden, Netherlands). Dopamine hydrochloride (DA), ±-norepinephrine hydrochloride (NE), Tris (hydroxymethyl) aminomethane hydrochloride (Tris-HCl), acetic acid, hydrochloric acid, sodium dodecyl sulfate (SDS), disodium hydrogen phosphate dihydrate, potassium chloride, sodium chloride, sodium dihydrogen phosphate, 4-(2-Hydroxyethyl) piperazine-1-ethanesulfonic acid (HEPES), sodium acetate trihydrate, polyoxyethylene sorbitan monoleate (Tween-20), 6-mercapto-1-hexanol (MCH), 11-mercaptoundecanoic acid (MUA), Human Serum Albumin (HSA), and sterile-filtered human serum from human male AB plasma (HS) were all purchased from Merck (Darmstadt, Germany). Serotonin hydrochloride (SE) and human IgG isotype control (catalogue #02–7102) were purchased from Thermo Fisher Scientific (Monza, Italy). Simulated Human Synovial Fluid (SF) was obtained from Biochemazone (Canada). 30K Amicon® Ultra centrifugal filter units were obtained from Millipore Corp. (Bedford, MA, USA). Ultrapure Milli-Q™ water (18.2 MΩ cm) was used to prepare all the buffer solutions. HBS-EP (10 mM HEPES, 150 mM NaCl, 3 mM EDTA, 0.005% Tween-20, pH 7.4) and PBS (140 mM NaCl, 2.68 mM KCl, 3.56 mM NaH_2PO_4, 6.44 mM Na_2HPO_4, pH 7.4), filtered through a microporous filter (0.22 μm Millipore filter), were used as

dilution and running buffer for the peptide and TNF-α protein in SPR analysis, respectively. SPR measurements were carried out by using Biacore X-100 instrumentation with bare gold sensor chips (SIA Au kit), provided by Cytiva AB (Uppsala, Sweden), further modified with the NTs-derived polymers.

2.2. Sensor chips preparation

Polymeric nanofilms of dopamine (PDA), norepinephrine (PNE), and serotonin (PSE) were directly formed on the SPR gold-coated sensor chip surface by applying a solution of 2.00 g L^{-1} of the functional monomer and 400 μmol L^{-1} of the peptide, as the imprinting template, in 10 mmol L^{-1} Tris-HCl pH 8.5 (or pH 9.5, only fo PSE) at 25.0 ± 0.5 °C for 5 h. The peptide chosen for polymers imprinting of TNF-α was selected following the approach previously reported (Baldoneschi et al., 2020b; Khumsap et al., 2021; Palladino et al., 2018; Pasquardini and Bossi, 2021; Torrini et al., 2021, 2022a, 2023a, 2023b). All the polymeric surfaces were finally passivated with a water/ethanol solution (80:20, v/v) of 1 mmol L^{-1} MUA and MCH, and finally washed with acetic acid (5% v/v) and deionized water to remove the template from the binding cavities of MIBPs. Non-imprinted polymers (NMIBPs) were prepared following the same experimental procedure except for template addition.

2.3. Evaluation of TNF-α peptide interaction with PDA/PNE/PSE-based MIBPs

The imprinting efficiency of the three different *MIBPs* based on PDA, PNE, or PSE versus the selected TNF-α peptide template was evaluated by performing a single cycle kinetic (SCK) analysis. It consisted of five sequential injections of increasing analyte concentration (3.75–60 μmol L^{-1}) diluted in HBS-EP pH 7.4 without performing the regeneration step among analyte (peptide or protein) injections. All the MIBPs surfaces were first tested with the peptide used as an imprinting template under the same conditions (i.e., peptide concentration and working buffer) by setting 120 s for the association and 30 s for the dissociation phase. Three measuring cycles were performed for each MIBP and, after each cycle, its surface was regenerated with a single-short injection (24 s) of 0.003% SDS, except for the PSE-based MIBP that was regenerated with 0.05% SDS (24 s). Data were processed by using Origin 2021b software by applying the 1:1 binding equation: $RU = R_{max} \times [Peptide]/(K_D + [Peptide])$ to the affinity calibration curve, where R_{max} is the maximum response (RU), and the K_D is the peptide-MIBP equilibrium dissociation constant. The kinetics (rate on = k_{on}; rate off = k_{off}) and affinity parameters ($K_D = k_d/k_a$) were also estimated by using the BIAEvaluation 3.1 Software (Cytiva, Sweden). The analytical parameters, namely limit of detection (LOD) and limit of quantitation (LOQ), were established respectively using the following equations: $LOD = 3\sigma \times K_D/R_{max}$ and $LOQ = 10\sigma \times K_D/R_{max}$, where sigma (σ) is the standard deviation of the mean signal of the blank solution.

2.4. PSE-based MIBPs for TNF-α monomer detection

PSE-based MIBPs prepared at pH 8.5 and 9.5 (see paragraph 2.2) were both used for the real time detection of the whole TNF-α protein by injecting 10 μL of the analyte from 12.5 nmol L^{-1} to 870 nmol L^{-1} (0.25 μg mL^{-1} - 15.0 μg mL^{-1}) in PBS pH 7.4 on the optical sensor surface (flow rate: 5 μL min^{-1}; temperature: 25.0 ± 0.05 °C). After each binding measurement the surface was regenerated with a single-short injection (2 μL) of SDS (0.06% and 0.08%). For each analyte concentration, three independent replicates were analyzed in manual run mode, and the calibration curve was constructed by plotting the mean values ± SD of the SPR responses against the standard solutions of the protein, and data elaborated with Origin 2021b software. In addition, kinetic/affinity parameters for TNF-α – MIBPs binding interactions were estimated by using the SCK protocol described in paragraph 2.3 within 12.5 nmol L^{-1} - 200 nmol L^{-1} (0.25 μg mL^{-1} - 3.80 μg mL^{-1}) concentration range for the analyte. Data processing was carried out using a linear regression fitting model and the sensitivity, expressed as LOD and LOQ were calculated according to the following equation: $LOD = 3\sigma/b$ and $LOQ = 10\sigma/b$, where sigma (σ) is estimated as the standard deviation expressed in concentration units of the measured signal for the blank, b (0 nmol L^{-1} TNF-α).

2.5. Selectivity of the PSE-based MIBPs

The efficiency of the imprinting process, in terms of selectivity against the target, was evaluated referring to the alpha (α) and the imprinting (IF) factors on both PSE-based MIBPs' surfaces (pH 8.5 and pH 9.5). The first factor was calculated according to the following equation:

$$\alpha = Q_{MIP\ target}/Q_{MIP\ competitor}$$

where Q is the mean value of SPR response obtained from three independent replicates of the target TNF-α/competitor proteins tested at a fixed concentration of 15.0 μg mL^{-1} in PBS, pH 7.4, as dilution/running buffer. HSA and IgG (abundant proteins in human serum) were used as potential interfering/competitor proteins, i.e. molecules able to non-specifically interact with the MIBP surface. The second factor, IF, calculated as MIBP/NIBP signal ratio, was estimated by injecting TNF-α monomer at a fixed concentration of 25 nmol L^{-1} (0.5 μg mL^{-1}) in buffer, for 120 s in manual run mode on both MIBPs and reference NIBPs surfaces to further evaluate possible nonspecific interactions.

2.6. TNF-α detection in human specimens by PSE-based MIBP

The detection of TNF-α by the PSE-based MIBP (pH 9.5) was also achieved in spiked SF and HS, clinically relevant human fluids for TNF-α diagnostics. SF was 1:50 diluted with PBS pH 7.4 and directly spiked with increasing TNF-α concentrations (25–870 nmol L^{-1}; 0.5–15.0 μg mL^{-1}). The analysis was conducted in manual run mode on the SPR platform, as reported for protein detection in buffer (flow rate: 5 μL min^{-1}; temperature: 25 °C). HS was fortified with the TNF-α protein considering two different concentration ranges: 25–870 nmol L^{-1} (0.5–15.0 μg mL^{-1}) "high level TNF-α" and 0.2–5.0 nmol L^{-1} (3–100 ng mL^{-1}) "low level TNF-α". All the spiked solutions were filtered by using 30K Amicon centrifugal devices according to the manufacturer's instructions (14,000×*g* for 10 min). "High level TNF-α" concentrations were directly injected into the SPR platform according to the manual run protocol reported above. "Low level TNF-α" samples were assayed according to a previously reported accumulation binding protocol to improve the detection limit in real matrices (Torrini et al., 2023a). Accordingly, the target analyte was injected by setting a total contact time of 1200 s, resulting from three sequential injections of 400 s each.

3. Results and discussion

3.1. Epitope imprinting of PSE and direct comparison with PDA and PNE

SE promises to be suitable to obtain green and "soft" bioinspired MIBPs similarly to the previous two, i.e., PDA and PNE (Baldoneschi et al., 2020a, 2020b; Battaglia et al., 2021, 2023; Palladino et al., 2018, 2019; Torrini et al., 2021, 2022a, 2022b, 2023a, 2023b). We first evaluated its ability to self-polymerize to polyserotonin (PSE) in very mild aqueous conditions and short time to produce MIBPs in presence of an amino acid-based template. Here, a short peptide sequence was used as an imprinting template, by following the same "epitope imprinting" approach previously reported (Baldoneschi et al., 2020b; Palladino et al., 2018; Torrini et al., 2021, 2022a, 2023a, 2023b). By this strategy, a suitable peptide is selected on the whole protein amino acid sequence. As a case study, here we selected the monomeric form of TNF-α as a relevant clinical biomarker. As sketched in Fig. 1A, on the whole

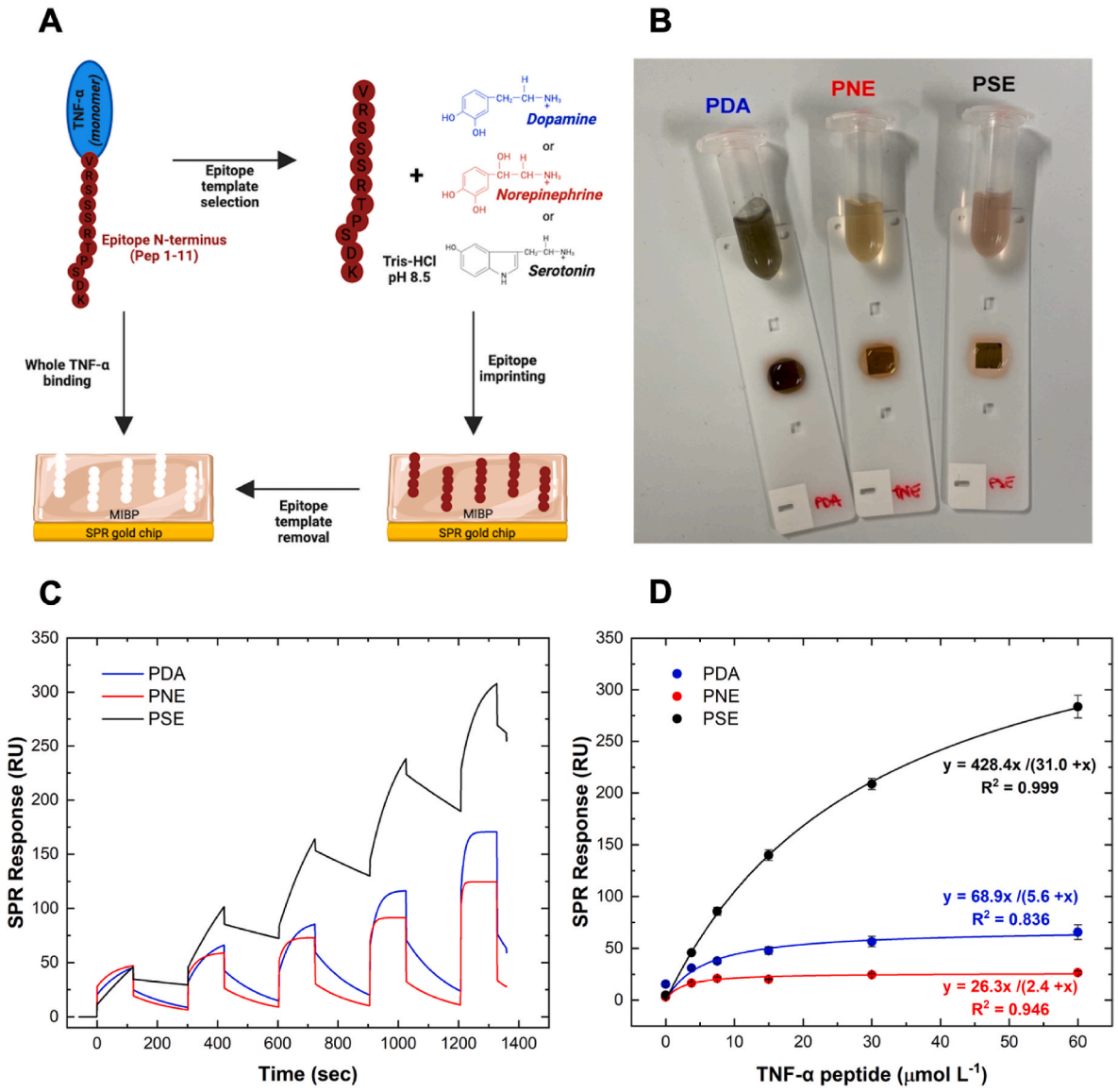

Fig. 1. (A) sketched procedure for epitope imprinting on PDA, PNE, and PSE; (B) polymerization solutions obtained by mixing DA, NE and SE with TNF-α peptide in Tris-HCl (pH 8.5) in vials and on gold chips at the end of the polymers' growth; (B) fitting of the SCK sensorgram with the 1:1 binding model obtained by injecting five increasing concentrations of TNF-α peptide in buffer (HBS-EP pH 7.4) on the three different MIBPs; (C) calibration curves of the TNF-α peptide obtained by Single Cycle Kinetic (SCK) within 3.75–60 μmol L^{-1}.

sequence, the 1–11 residues (VRSSSRTPSDK; MW = 1218.33 Da) were chosen as the epitope sequence for imprinting. The N-terminal position, together with other physicochemical considerations, is generally able to guarantee a good imprinting efficiency in these NTs-based MIBPs due to a high freedom degree and the absence of secondary structures. The MIBP growth, performed in 5 h at 25 °C in presence of the peptide, leads to the formation of an auto-assembled and adherent nanofilm directly on the SPR gold chip surface (Fig. 1A and B).

The advantages of this approach are numerous: the synthesis cost is significantly reduced; the process is simplified to a one step synthesis, and it is completely green; the washing out of the peptide from the polymer matrix is easily and effectively achieved by a washing step with acetic acid. The MIBPs produced are durable and stable and can be reused for a high number of measurements, after regeneration. SPR was employed as a reference platform to evaluate the main analytical performances of the PSE-based MIBPs in terms of affinity binding toward the target analyte.

For direct comparison, PDA- and PNE-based MIBPs were also synthesized and tested in parallel with those prepared starting from PSE by SPR and SCK (Fig. 1C and D). The peptide used as template epitope was first used as the calibrator in buffer conditions (3.75–60 μmol L^{-1}), and the specific binding features of the three MIBPs were evaluated in terms of kinetic rates (k_{on}/k_{off}), equilibrium constants (K_D), and R_{max} (Table 1).

As reported in the Table, the highest theoretical binding value was obtained for the PSE-based MIBP ($R_{max} = 2.8 \pm 0.4 \times 10^2$), with respect

Table 1
kinetic (k_{on}/k_{off}) and affinity (K_D) constants inferred by SPR experiments with NTs-based MIBPs. Values are relative to gold chips modified with the three different polymers (PDA, PNE and PSE). Standard peptide solutions are tested in HBS-EP buffer in a 3.75–60 μmol L^{-1} concentration range.

Polymers	k_{on} (1/Ms)	k_{off} (1/s)	K_D (μmol L^{-1})	R_{max}
PDA	$1.3 \pm 0.1 \times 10^3$	$7 \pm 1 \times 10^{-3}$	5.2 ± 0.6	$9 \pm 1 \times 10^1$
PNE	$3.0 \pm 0.5 \times 10^3$	$7 \pm 3 \times 10^{-3}$	2.2 ± 0.6	37 ± 7
PSE	$3.4 \pm 0.2 \times 10^2$	$9.1 \pm 0.5 \times 10^{-4}$	2.7 ± 0.3	$2.8 \pm 0.4 \times 10^2$

to the other two functional monomers, DA and NE, which exhibited a much lower capture capacity toward the target. Specifically, the imprinting of PDA and PNE resulted in lower R_{max} responses, of about 3 and 8 folds, respectively (Fig. 1C and D). Since R_{max} is primarily related to the receptor surface saturation (and thus to the surface density of the active recognition cavities), the results obtained by using PSE could thus suggest that this polymer is likely able to establish a greater number of affinity interactions during the co-polymerization step between the monomer and the peptide template (keeping constant the template molarity). This in turn elicits a higher surface density in terms of recognition cavities, and thus in terms of a higher binding capacity and R_{max} value. The K_D value of the PSE-based MIBP, at least with this selected epitope sequence, resulted very similar to the PNE-based one, and both were lower than the K_D value of PDA-based MIBP. However, looking at the kinetic rates (k_{on} and k_{off}) it is worth noting that PSE-based MIBP displays a rate of dissociation about one order of magnitude slower than PNE-based MIBP, reinforcing the hypothesis that PSE can establish stronger and more stable affinity interactions with the peptide sequence both during co-polymerization and binding. This undoubtedly deserves to be consolidated by other case studies in the next future. The PSE-based biosensor exhibited also the best analytical performances, in terms of dynamic range of the calibration, repeatability ($_{av}$CV%), and sensitivity (LOD and LOQ). Fig. 1D shows the excellent correlation coefficient ($R^2 = 0.999$) obtained, compared to the other two MIBPs (R^2 = 0.836 and 0.946 for PDA and PNE, respectively). The repeatability of the measurements, $_{av}$CV%, was also excellent for the PSE-based MIBP (3.1%), while significantly lower for PDA (8.2%) and PNE (9.4%). This could be likely related to the higher hydrophilicity of PSE, compared to PDA and PNE (Ishino et al., 2022), able to improve both the binding and the removal steps during SPR measurements. Also LOD and LOQ values (22 ± 1 nmol L^{-1} and 72 ± 3 nmol L^{-1}, respectively) resulted improved for the PSE-based MIBP, respect to those obtained with PDA and PNE-based MIBPs (LOD = 410 ± 40 nmol L^{-1} (LOQ = 1.4 ± 0.1 μmol L^{-1}) and LOD = 300 ± 30 nmol L^{-1} (LOQ = 990 ± 1 nmol L^{-1}), respectively), confirming the better binding capacity of PSE with respect to the other polymers for the selected analyte.

These first results show that PSE can be successfully polymerized and imprinted by an "epitope" approach, similarly to PDA and PNE, sharing with the previous two NT monomers not only the ability of auto-polymerizing and self-adhering under the same conditions, but also the natural propensity of interacting with peptide sequences to create 3D surface recognition cavities with reversible binding features. Moreover, at least in this first case study, this new and promising polymer showed a dramatic improvement in the RU responses and in all the analytical performances of the biosensor (except for K_D that resulted in line with that of PNE).

3.2. Effect of pH on imprinted PSE growth and its binding ability

To allow a direct comparison of the three polymers, we first synthesized PSE-based MIBPs under the same imprinting conditions previously set up for PDA and PNE, *i.e.*, aqueous solution at pH 8.5. Once drawn the main features of the new imprinted polymer (paragraph 3.1), we also considered the experimental conditions recently reported for the synthesis of PSE nanoparticles, performed in phosphate buffer at pH 9.5 (Ishino et al., 2022). As explained by authors, SE shows a much slower self-polymerization rate than DA and NE under the same reaction conditions (Meng et al., 2022), and a more basic pH improves the process. Thus, the PSE-MIBP synthesis was repeated both at pH 8.5 and 9.5 (PSE@pH8.5 and PSE@pH9.5) using the same epitope-mediated imprinting reported above but by assaying the TNF-α monomer protein as a calibrator by SPR (instead of the epitope peptide itself). As reported in Fig. 2, both the MIBPs were able to efficiently bind the TNF-α monomer in a concentration-dependent manner, allowing the SPR biosensor to reach a LOD of 1.05 ± 0.07 nmol L^{-1} (18 ± 1 ng mL^{-1}) for PSE@9.5 and 2.6 ± 0.2 nmol L^{-1} (45 ± 3 ng mL^{-1}) for PSE@8.5. Both the LODs obtained by calibrating the biosensor with TNF-α protein resulted in an improvement of more than one order of magnitude with respect to the LOD obtained by calibrating the epitope template as a target (22 ± 1 nmol L-1). This is due to the increased refractive index change when the whole protein binds the MIBP surface, related to the higher molecular weight of the protein with respect to the short peptide template and confirms the ability of the MIBP in binding the whole protein. The TNF-α protein binding demonstrates the effectiveness of the epitope-imprinting approach used to generate the PSE-based MIBP. The $_{av}$CVs% resulted very good under both the pH polymerization conditions, i.e., 4.2% for PSE@9.5 and 6.6% for PSE@8.5. The binding affinity between the target protein and MIBPs surfaces, assayed by the SCK protocol (see Fig. 2A and paragraphs 2.3 and 2.4) allowed to draw a linear fitting within the tested concentration range in both the cases, with correlation coefficients (R^2) of 0.991 and 0.985, respectively (Fig. 2B).

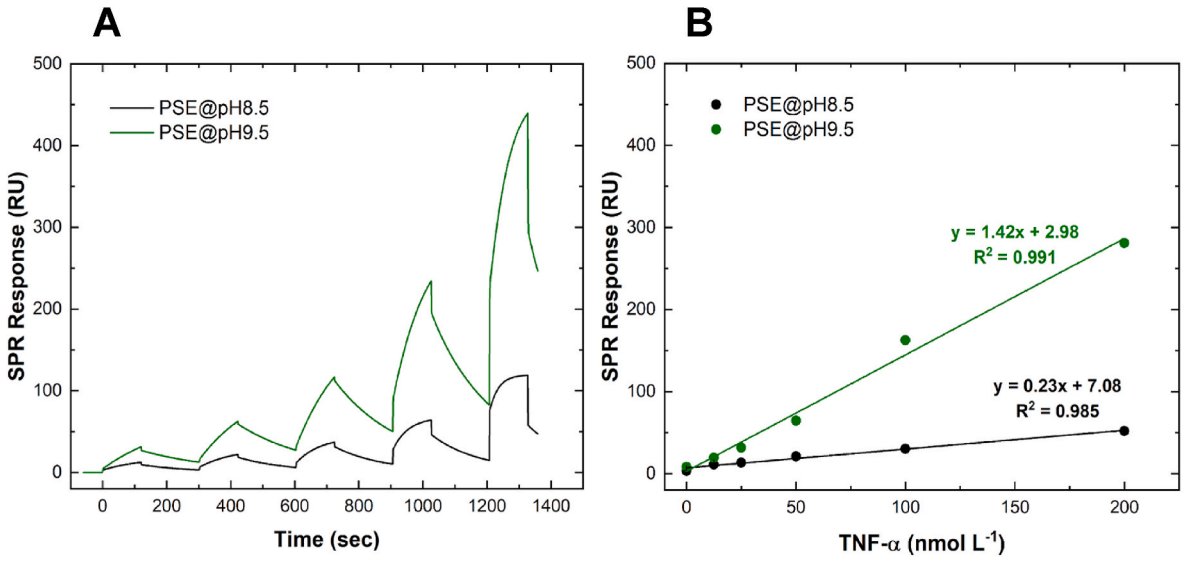

Fig. 2. (A) fitting of the SCK sensogram with the 1:1 binding model obtained by injecting five increasing concentrations of TNF-α protein in buffer (PBS pH 7.4) on MIBPs PSE@8.5 (black line) and PSE@9.5 (green line); (B) calibration curves by Single Cycle Kinetic (SCK) analysis performed with the TNF-α whole protein (12.5–200 nmol L^{-1}; 0.25–3.80 μg mL^{-1}) with two different MIBPs: PSE@8.5 (black line) and PSE@9.5 (green line). Error bars represent standard deviations (n = 3).

The K_D value of PSE@8.5 resulted 43.7 ± 0.2 nmol L^{-1}, while that of PSE@9.5 79 ± 10 nmol L^{-1}, showing a two folds improvement under milder basic pH, which is also the most reported value for PDA and PNE polymerization in the literature. Contrarily, a dramatic increment in terms of surface saturation, i.e., R_{max}, emerged by preparing the MIBP at pH 9.5 (445 ± 2 RU vs 72 ± 2 RU), leading to a 6 fold increase of this key parameter. This may be linked to the higher rate of PSE polymerization at pH 9.5, which could positively impact on the number of binding cavities available for the specific interaction with the target protein but deserves further study and morphological characterization of the polymer to be fully explained. We recently demonstrated (Torrini et al., 2023a) how important is the R_{max} parameter of a MIBP surface in SPR, mainly when dealing with very low target concentration levels in untreated and complex biological matrices. In fact, it allows to perform a simple and direct analyte accumulation on the receptor surface to amplify the specific signal, as also reported here for TNF-α in human serum (paragraph 3.4). The pH of the monomer-template solution impacts the epitope-imprinting polymerization process, since a proper electrostatic environment during the co-polymerization of SE (or DA and NE) and the epitope peptide is necessary. Then, to achieve an efficient imprinting, net opposite charges (negative for the polymer and positive for the peptide) should be assured during the process. This means that the suitable pH is the one at which, at the same time, the epitope is positively charged, and the polymer is negatively charged, respectively. A suitable pH choice is thus restricted above the isoelectric point (IP) of the polymer and below that of the selected epitope sequence. This consideration is also valid when bulk imprinting is used i.e., with the whole protein.

3.3. Selectivity of the PSE-based MIBPs

The binding selectivity of the two PSE-based MIBPs (PSE@9.5 MIBP and PSE@8.5 MIBP) was first evaluated by testing, separately, the two most abundant proteins in human serum, *i.e.* Human Serum Albumin (HSA) and the major immunoglobulin class (IgG), which could be the main source of non-specific interactions during TNF-α analysis in real matrices. Protein solutions in PBS buffer pH 7.4 were tested at 15.0 μg mL^{-1} and all the SPR signals (RU) recorded were then normalized with respect to the molecular weight (RU/MW) to consider the different MWs between the tested proteins (HSA = 66500 Da and IgG = 150000 Da). According to the guidelines for the interpretation of the α factor parameter (Battaglia et al., 2023; Mostafa et al., 2021; see also paragraph 2.5), that resulted always widely >1, both the MIBPs (PSE@9.5 and PSE@8.5) displayed excellent selectivity toward the target protein (Fig. 3). Noteworthy, even if the PSE@9.5 MIBP showed a slightly worse selectivity respect to PSE@8.5 MIBP, it displayed a marked higher performance in terms of SPR signal intensity, likely due to the higher recognition cavities surface density as discussed above.

To extend the evaluation of the selectivity of the SPR biosensor, the so-called Imprinting Factor (IF) was also estimated by testing TNF-α protein on non-imprinted PSE polymers (NMIBP), at both pH 8.5 and 9.5. IF, complementary to the α factor, estimates the interaction of the analyte/matrix components with the non-imprinted surface possibly occurring with a polymeric surface, and how the imprinting process addresses the analyte binding selectively. It is calculated as the RU_{MIBP}/RU_{NMIBP} ratio. Here, a solution of TNF-α (25 nmol L^{-1} (0.5 μg mL^{-1}) in buffer) is added to both MIBP and NMIBP to infer possible non-specific interactions of the analyte. As a result, a considerable gain in the specific binding of TNF-α was obtained for PSE imprinted at pH 9.5 (IF = 6.2, vs IF = 3.4 for PSE@8.5).

Based on all the results obtained, we decided to move to TNF-α detection and quantification in biological matrices by selecting the PSE@pH9.5 MIBP, in accordance with its best analytical performance in terms of SPR signal intensity, repeatability, linearity, and sensitivity.

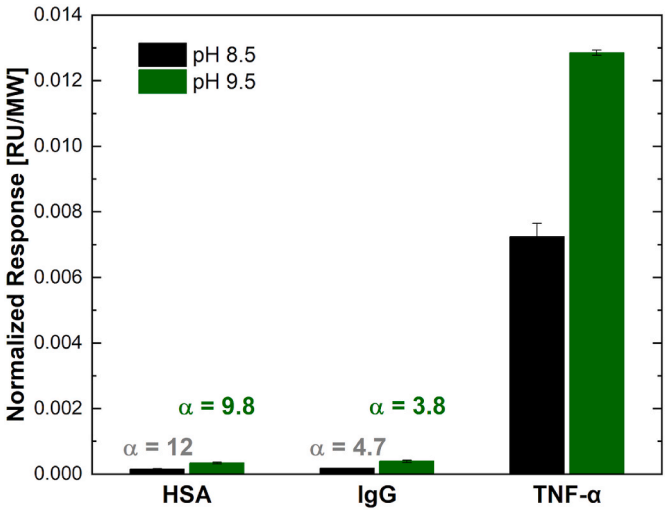

Fig. 3. Comparison of the SPR responses for HSA and IgG with the target protein (TNF-α) tested at a fixed concentration (15.0 μg mL^{-1}) in buffer on the PSE-based MIPs imprinted at different pHs (pH 8.5 (black), pH 9.5 (green)). The RU_{mean} ± SD were calculated for independent triples for each protein as well as for TNF-α. The α values were calculated for both the PSE-based MIPs (PSE@pH8.5 and PSE@pH9.5) against HSA and IgG. All the values were calculated according to the equation $\alpha = Q_{MIP\ target}/Q_{MIP\ competitor}$, where Q is the mean value of SPR responses recorded for the interactions of the two PSE-based MIBPs modified Au chips.

3.4. TNF-α detection in human specimens by PSE-based MIBP

TNF-α is one of the most potent multifunctional pro-inflammatory cytokines, playing a pivotal role in many infectious and inflammatory pathologies. Therefore, its measurement in human fluids, such as saliva, tears, urine, synovial fluid, plasma, and serum is necessary, and might be helpful in the staging and prognosis of diseases (Idriss and Naismith, 2000; Liu et al., 2021; Lu et al., 2021). However, the values of physiological/pathological ranges of the biomarker differ according to the analyzed matrix and could be influenced by the several conditions and disorders. For example, the synovial fluid, a straw-coloured liquid found in small amounts in joints, is the targeting matrix for monitoring and assessing rheumatoid arthritis (RA) disease. There are several pieces of evidence that identify the TNF-α as an important biomarker for joint disorders and increasing levels to 29 pmol L^{-1} (500 pg mL^{-1}) were found in patients (Santos-Savio et al., 2015; Vasanthi et al., 2007). On the other hand, the TNF-α concentration in the serum of healthy humans is lower than 0.1 pmol L^{-1} (2.0 pg mL^{-1}) and increases to about 1.7–2.3 pmol L^{-1} (30.0–40.0 pg mL^{-1}) in the serum of patients with severe autoimmune diseases (Liu et al., 2021; Oliver et al., 1993). Serum TNF-α concentrations up to 9.8 pmol L^{-1} (170.0 pg mL^{-1}) were found in patients with Parkinson's disease, and even higher in patients with septic shock (290 pmol L^{-1}; 5000 pg mL^{-1}), indicating important inhomogeneity among different pathogenic conditions (Damas et al., 1989; El-Kattan et al., 2022). Other body fluids, *i.e.*, saliva, urine, and tears have recently received increasing attention because they are easy to be sampled in a non-invasive way and have a less complex biological composition. Nevertheless, the level of TNF-α in these matrices is extremely low (0.6–1.7 pmol L^{-1}; 10.0–30.0 pg mL^{-1}) compared to synovial fluid or serum (Carreño et al., 2010; Liu et al., 2021; Lu et al., 2021). On this basis, we decided to assay TNF-α in synovial fluid and human serum as clinically relevant matrices, to evaluate the applicability of the new PSE-based MIBP biosensor in a real case of interest. SF and HS were fortified with increasing TNF-α concentration (25 nmol L^{-1} - 870 nmol L^{-1}; 0.5–15.0 μg mL^{-1}), as previously tested in buffer solution. The SPR response to blank HS/HF (without TNF-α) was independently checked to estimate any matrix contribution, obtaining a very

low nonspecific binding (13.0 ± 0.3 RU) and a α-factor value of 2.2, considering the lowest spiked analyte concentration.

As reported in Fig. 4, the biosensor successfully responded to increasing concentrations of the analyte both in SF and HS, displaying a higher sensitivity (LOD = 2.8 ± 0.2 vs 4.5 ± 0.6 nmol L^{-1} and LOQ = 9.4 ± 0.5 vs 15 ± 2 nmol L^{-1}) and a wider linear range in HS within the concentration range investigated. A better repeatability was obtained in SF with respect to HS ($_{av}$CV% = 2.8 vs 6.3%).

The ability in achieving efficient and direct TNF-α quantitative detection in HS represents a very encouraging result not only as the first application of imprinted PSE to SPR biosensing, but also for its potential application to mini invasive sampling, compared to SF specimen collection, which is harvested by arthrocentesis from patients. HS is also less prone to variability in analyte composition due to sample storage, even in the case of short-term room temperature or refrigerated stockage (Gislefoss et al., 2009; Kapuruge et al., 2022). Moreover, assaying TNF-α in HS is of great interest for the diagnosis of a number of important diseases (e.g. cancer, heart disease, sepsis, rheumatoid arthritis, etc), commonly quantified by immuno-based assays designed to measure the target biomarker in serum or plasma (Breen et al., 2011; Chiswick et al., 2012; Dupuy et al., 2013; Jones and Singer, 2001; Kartikasari et al., 2021; Nechansky et al., 2008; Valaperti et al., 2020; Wang et al., 2006). In addition, the analysis of TNF-α in blood specimens can provide highly valuable clinical information to measure the pathological status of the patients and to adjust therapies in different inflammatory diseases (Jang et al., 2021; Liu et al., 2021). However, since the concentration levels of TNF-α in HS span from tens of pg mL^{-1} to ng mL^{-1}, depending on the considered disease, we moved on to improve the sensitivity obtained in HS by standard analysis protocol, which is unsatisfactory for clinical application. We thus modified the analysis protocol by performing an on-chip accumulation step of the analyte, as very recently demonstrated for PD-L1 quantification in HS by SPR (Torrini et al., 2023a). The protocol consists in a prolonged injection (see paragraph 2.6 for details) of the sample on the PSE MIBP to favor the surface accumulation of the target protein. To this aim, a high R_{max} value and a good selectivity are the key features of the MIBP that should be privileged to avoid valuable and reliable signal enhancement, as previously mentioned in paragraph 3.2. This simple procedure greatly impacted on the TNF-α LOD, which was lowered down to 21 ± 4 pmol L^{-1} (360 ± 70 pg mL^{-1}), with R^2 = 0.988 and an excellent assay repeatability of $_{av}$CV% = 1.5% (Fig. 5). From a clinical point of view, the final LOD obtained is consistent with the sensitivity reported for commercially available immunoassays and sensors, mainly involving antibodies for detection (Chiswick et al., 2012; Filik and Avan, 2020; Ghosh et al., 2018; Jeong et al., 2013; Kartikasari et al., 2021; Li et al., 2021; Valaperti et al., 2020; Wang et al., 2006). Anyway, prospect work could be dedicated to further improve the detection limit by optimizing amplification strategies, e.g. by using imprinted polymers nanoparticles to develop a completely antibody-free sandwich assay.

4. Conclusions

Here it is presented the first and successful use of the natural neurotransmitter serotonin (SE) as a functional monomer for imprinted "soft" biopolymers of the new generation, able to replace the use of traditional antibodies in bioassays. Following the exciting results previously obtained by using PDA and PNE, this is the third NT-based functional monomer that is of great interest for the effective capturing of large biomolecules. As the previous two, the preparation protocol is fast, completely green, low cost, and its self-polymerization leads to auto-adhesive nanofilms that can be efficiently coupled to a large variety of supports, SPR gold biochips in this work. As the first model study, we selected the detection and quantification of a clinical biomarker of relevance in several diseases diagnosis and clinical follow up, i.e., serum TNF-α. However, we also demonstrated that the MIBP can effectively detect the protein in synovial fluid, since TNF-α clinical levels of interest span within a wide concentration range. The direct comparison of the analytical performances of the PSE-based biosensor with those of imprinted polymers prepared starting from DA and NE showed improved sensitivity and higher binding capability for the target analyte. Specifically, the imprinting of PDA and PNE resulted in higher detection limits of about 20 and 13 folds, respectively. Moreover, the selectivity of the biosensor coated with the new PSE polymer turned out excellent, showing the ability in discriminating the target protein over the major interfering proteins commonly present in human matrices (e.g. HSA and IgG). Finally, the TNF-α calibration was successfully achieved in real human serum with a low picomolar sensitivity (LOD = 21

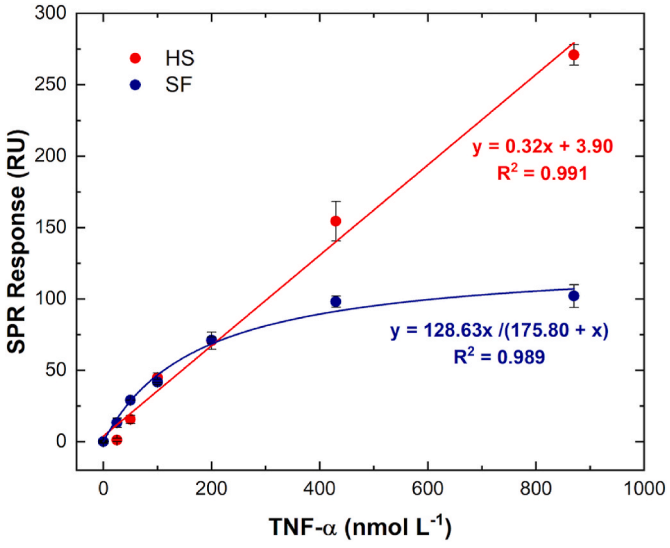

Fig. 4. Response of PSE@pH9.5 based biosensor at increasing concentration (25–870 nmol L^{-1}; 0.5–15.0 μg mL^{-1}) of TNF-α in human serum (HS) (red line) and synovial fluid (SF) (blue line). The SPR signal of the blank matrices was subtracted from each measurement. The results are reported as the mean value of three independent replicates for each concentration injection. Each injection was followed by a regeneration step (manual run mode).

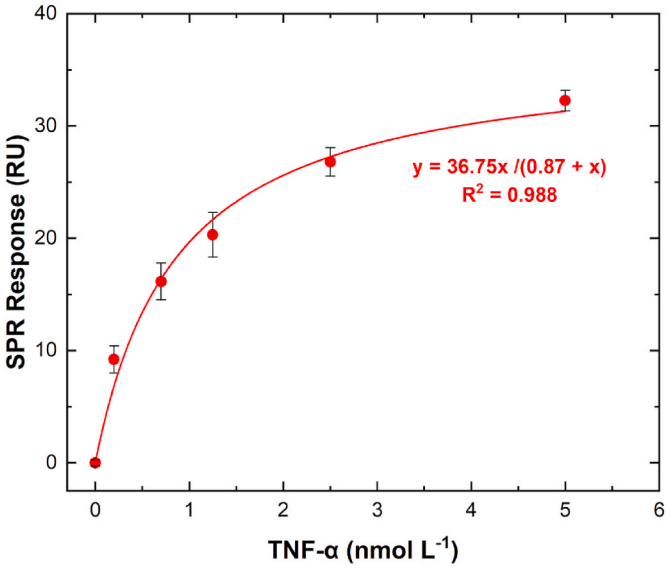

Fig. 5. *calibration curve of MIBP response to different concentrations of TNF-α in spiked HS (0.2 – 5.0 nmol L^{-1}; 3–100 ng mL^{-1}) according to the accumulation binding approach. The SPR signal of the blank matrix was subtracted from each measurement. The results are reported as the mean value of three independent replicates for each concentration injection. Each injection was followed by a regeneration step (manual run mode).*

$\pm$ 4 pmol L^{-1}; 360 $\pm$ 70 pg mL^{-1}) and excellent reproducibility ($_{av}$CV% = 1.5%). These results appear very promising for the next future of imprinted PSE for bioanalytical assays when used as a biomimetic receptor, particularly suitable for the detection of peptides and proteins. From the perspective of clinical and diagnostic applications, the challenge will be to improve the biosensor sensitivity to be more competitive with commercial immunoassays, and to cover the clinically relevant range of concentrations in several conditions and diseases.

Declaration of competing interest

The authors declare that they have no known competing financial interests or personal relationships that could have appeared to influence the work reported in this paper.

Data availability

Data will be made available on request.

Acknowledgments

S. Scarano and F. Battaglia thank the Ministry of Education, University and Research (MIUR) for the scientific program SIR2014 Scientific Independence of young Researchers (RBSI1455LK). S. Scarano and F. Torrini thank the project 'Biocompatible Molecularly Imprinted Polymers as alternative to antibody-based therapy for Rheumatoid Arthritis treatment, MIPRA' funded by the Fondazione Roche per la Ricerca Indipendente (Rome). The authors also thank the Italian Ministry of University and Research (MUR), for the project "Dipartimenti di Eccellenza 2023–2027".

References

Arabi, M., Ostovan, A., Li, J., Wang, X., Zhang, Z., Choo, J., Chen, L., 2021. Adv. Mater. 33 (30), 2100543.
Arad-Yellin, R., Hudák, A., Letoha, T., Green, B.S., 2023. Eur. J. Med. Chem. 8, 100106.
Balayan, S., Chauhan, N., Kumar, P., Chandra, R., Jain, U., 2022. 3 Biotech. 12 (1), 37.
Baldoneschi, V., Palladino, P., Scarano, S., Minunni, M., 2020a. Anal. Bioanal. Chem. 412, 5945–5954.
Baldoneschi, V., Palladino, P., Banchini, M., Minunni, M., Scarano, S., 2020b. Biosens. Bioelectron. 157, 112161.
Battaglia, F., Baldoneschi, V., Meucci, V., Intorre, L., Minunni, M., Scarano, S., 2021. Talanta 230, 122347.
Battaglia, F., Bonelli, F., Sgorbini, M., Intorre, L., Minunni, M., Scarano, S., Meucci, V., 2023. Anal. Methods 15, 27–35.
Breen, E., Reynolds, S.M., Cox, C., Jacobson, L.P., Magpantay, L., Mulder, C.B., Dibben, O., Margolick, J.B., Bream, J.H., Sambrano, E., Martínez-Maza, O., Sinclair, E., Borrow, P., Landay, A.L., Rinaldo, C.R., Norris, P.J., 2011. Clin. Vaccine Immunol. 18, 1229–1242.
Carreño, E., Enríquez-de-Salamanca, A., Tesón, M., García-Vázquez, C., Stern, M.E., Whitcup, S.M., Calonge, M., 2010. Acta Ophthalmol. 88 (7), e250–e258.
Checco, J.W., Eddinger, G.A., Rettko, N.J., Chartier, A.R., Gellman, S.H., 2020. ACS Chem. Biol. 15 (8), 2116–2124.
Chiswick, E.I., Duffy, E., Japp, B., Remick, D., 2012. Methods Mol. Biol. 844, 15–30.
Corti, A., Fassina, G., Marcucci, F., Barbanti, E., Cassani, G., 1992. Biochem. J. 284 (Pt 3), 905–910.
Damas, P., Reuter, A., Gysen, P., Demonty, J., Lamy, M., Franchimont, P., 1989. Crit. Care Med. 17 (10), 975–978.
Daub, H., Traxler, L., Ismajli, F., Groitl, B., Itzen, A., Rant, U., 2020. Sci. Rep. 10, 9265.
Dupuy, A., Kuster, N., Lizard, G., Ragot, K., Lehmann, S., Gallix, B., Cristol, J., 2013. Clin. Chem. Lab. Med. 51, 1–9.
El-Kattan, M.M., Rashed, L.A., Shazly, S.R., Ismail, R.S., 2022. Egypt J. Neurol. Psychiatry Neurosurg. 58, 25.
Filik, H., Avan, A.A., 2020. Talanta 211, 120758.
Ghosh, S., Datta, D., Chaudhry, S., Dutta, M., Stroscio, M.A., 2018. IEEE Trans. NanoBioscience 17, 417–423.
Gislefoss, R.E., Grimsrud, T.K., Mørkrid, L., 2009. Clin. Chem. Lab. Med. 47 (5), 596–603.
Hlodan, R., Pain, R.H., 1995. Eur. J. Biochem. 231, 381–387.
Horiuchi, T., Mitoma, H., Harashima, S., Tsukamoto, H., Shimoda, T., 2010. Rheumatology 49, 1215–1228.
Idriss, H.T., Naismith, J.H., 2000. Microsc. Res. Tech. 50 (3), 184–195.
Ishino, K., Nishitani, S., Man, Y., Saito, A., Sakata, T., 2022. Langmuir 28, 8633–8642.
Jang, D., Lee, A.-H., Shin, H.-Y., Song, H.-R., Park, J.-H., Kang, T.-B., Lee, S.-R., Yang, S.-H., 2021. Int. J. Mol. Sci. 22, 2719.
Jeon, K., Andoy, N.M.O., Schmitt, C.W., Xue, Y., Barner, L., Sullan, R.M.A., 2021. J. Mater. Chem. B 9, 634–637.
Jeon, K., Asuncion, J.A., Corbett, A.L., Yuan, T., Patel, M., Andoy, N.M.O., Kreis, C.T., Voznyy, O., Sullan, R.M.A., 2022. Nanomaterials 12, 2027.
Jeon, Y.J., Kang, S.M., 2013. Polym. Degrad. Stabil. 98, 1271–1273.
Jeong, H.-H., Erdene, N., Park, J.-H., Jeong, D.-H., Lee, H.-Y., Lee, S.-K., 2013. Biosens. Bioelectron. 39, 346–351.
Jones, L.J., Singer, V.L., 2001. Anal. Biochem. 293, 8–15.
Kapuruge, E.P., Jehanathan, N., Rogers, S.P., Williams, S., Chung, Y., Borges, C.R., 2022. Mol. Cell. Proteomics 21 (11), 100420.
Kartikasari, A.E.R., Huertas, C.S., Mitchell, A., Plebanski, M., 2021. Front. Oncol. 11, 692142.
Khumsap, T., Corpuz, A., Nguyen, L.C., 2021. RSC Adv. 11, 11403–11414.
Kiratitanavit, W., Bruno, F.O., Xia, Z., Yu, S., Kumar, J., Nagarajan, R., 2019. J. Renew. Mater. 7, 205–214.
Lee, H., Dellatore, S.M., Miller, W.M., Messersmith, P.B., 2007. Science 318, 426–430.
Li, H., Li, X., Chen, L., Li, B., Dong, H., Liu, H., Yang, X., Ueda, H., Dong, J., 2021. ACS Omega 6, 31009–31016.
Liu, C., Chu, D., Kalantar-Zadeh, K., George, J., Young, H.A., Liu, G., 2021. Adv. Sci. 8 (15), e2004433.
Lu, Y., Zhou, Q., Xu, L., 2021. Bioeng. Biotechnol. 9, 701045.
Madikizela, L.M., Tavengwa, N.T., Tutu, H., Chimuka, L., 2018. Trends Environ. Anal. Chem. 17, 14–22.
Martín-Esteban, A., 2013. Trends Environ. Anal. Chem. 45, 169–181.
Meng, Y., Zhu, J., Dinga, J., Zhou, W., 2022. Chem. Commun. 58, 6713–6716.
Mostafa, A.M., Barton, S.J., Wren, S.P., Barker, J., 2021. Trends Anal. Chem. 144, 116431.
Nakatsuka, N., Hasani-Sadrabadi, M.M., Cheung, K.M., Young, T.D., Bahlakeh, G., Moshaverinia, A., Weiss, P.S., Andrews, A.M., 2018. ACS Nano 5, 4761–4774.
Nechansky, A., Grunt, S., Roitt, I.M., Kircheis, R., 2008. Biomark. Insights 3, 227–235.
Oliver, J.C., Bland, L.A., Oettinger, C.W., Arduino, M.J., McAllister, S.K., Aguero, S.M., Favero, M.S., 1993. Lymphokine Cytokine Res. 12 (2), 115–120.
Ostovan, A., Arabi, M., Wang, Y., Li, J., Li, B., Wang, X., Chen, L., 2022. Adv. Mater. 34 (42), 2203154.
Palladino, P., Minunni, M., Scarano, S., 2018. Biosens. Bioelectron. 106, 93–98.
Palladino, P., Bettazzi, F., Scarano, S., 2019. Anal. Bioanal. Chem. 411, 4327–4338.
Pasquardini, L., Bossi, A.M., 2021. Anal. Bioanal. Chem. 413, 6101–6115.
Popa, C., Netea, M.G., van Riel, P.L.C.M., van der Meer, J.W.M., Stalenhoef, A.F.H., 2007. J. Lipid Res. 48 (4), 751–762.
Ryu, J.H., Messersmith, P.B., Lee, H., 2018. ACS Appl. Mater. Interfaces 10 (9), 7523–7540.
Santos Savio, A., Machado Diaz, A.C., Chico Capote, A., Miranda Navarro, J., Rodrìguez Alvarez, Y., Bringas Pérez, R., Estévez del Toro, M., Guillen Nieto, G.E., 2015. BMC Muscoskel. Disord. 16, 51.
Torrini, F., Palladino, P., Baldoneschi, V., Scarano, S., Minunni, M., 2021. Anal. Chim. Acta 1161, 338481.
Torrini, F., Battaglia, F., Palladino, P., Scarano, S., Minunni, M., 2022a. Biosens. Bioelectron. 217, 114706.
Torrini, F., Caponi, L., Bertolini, A., Palladino, P., Cipolli, F., Saba, A., Paolicchi, A., Scarano, S., Minunni, M., 2022b. Anal. Bioanal. Chem. 414, 5423–5434.
Torrini, F., Goletta, G., Palladino, P., Scarano, S., Minunni, M., 2023a. Biosens. Bioelectron. 220, 114806.
Torrini, F., Battaglia, F., Sestaioni, D., Palladino, P., Scarano, S., Minunni, M., 2023b. Sensor. Actuator. B Chem. 383, 133586.
Valaperti, A., Li, Z., Vonow-Eisenring, M., Probst-Müller, E., 2020. J. Pharm. Biomed. Anal. 179, 113010.
van Schie, K.A., Ooijevaar-de Heer, P., Dijk, L., Kruithof, S., Wolbink, G., Rispens, T., 2016. Sci. Rep. 6, 32747.
Vasanthi, P., Nalini, G., Rajasekhar, G., 2007. APLAR J. Rheumatol. 10 (4), 270–274.
Wang, J., Liu, G.D., Engelhard, M.H., Lin, Y.H., 2006. Anal. Chem. 78, 6974–6979.
Xie, C., Wang, X., He, H., Ding, Y., Lu, X., 2020. Adv. Funct. Mater. 30 (25), 1909954.
Yang, J.C., Lim, S.J., Cho, C.H., Hazarika, D., Park, J.P., Park, J., 2023. Sensor. Actuator. B Chem. 390, 133982.
Zaidi, S.A., 2019. ChemistrySelect 4, 5081–5090.